This is a preprint, the final version is subject to change, of the American Mineralogist (MSA)
Cite as Authors (Year) Title. American Mineralogist, in press.
DOI: http://dx.doi.org/10.2138/am-2018-6137

A Manuscript Celebrating the Centennial of the America Mineralogist

The Third Isotope of the Third Element on the Third Planet

Revision 1, 27-September-2017

by

Douglas Rumble

drumble@carnegiescience.edu

Geophysical Laboratory, 5251 Broad Branch Rd., NW, Washington, DC, 20015

Abstract

The third isotope of the third element, ^{17}O, records indispensible information on the origin and operation of Earth, the third planet. The measured uniformity in fractionation of ^{16}O, ^{17}O and ^{18}O in rocks and minerals over the whole of geologic time, from Hadean to Recent, records the existence of a global magma ocean prior to the formation of continents. New techniques of high-resolution mass spectroscopy and of femtosecond X-ray diffraction are leading towards a deep understanding of the origin of kinetic isotope fractionation effects during metabolism. Analysis for the rare molecule $^{17}O^{18}O$, distinguished by the substitution of two heavy isotopes, in combination with data on $^{18}O^{18}O$, provides an insight into the mechanism whereby plants produce oxygen. Given the skills of American Mineralogist readers in three-dimensional visualization of complex crystalline and molecular structures and the talents of biogeochemical colleagues in measuring isotope fractionation by organisms in nature, there is every

This is a preprint, the final version is subject to change, of the American Mineralogist (MSA)
Cite as Authors (Year) Title. American Mineralogist, in press.
DOI: http://dx.doi.org/10.2138/am-2018-6137

reason to expect extraordinary advances in understanding the cycling of life's elements, H, C, N, O, and S between the biosphere, atmosphere, hydrosphere, and lithosphere.

Introduction

Oxygen, the third most abundant element in the Solar System, after hydrogen and helium, occupies most of the volume of silicate and oxide minerals in Earth's crust and mantle. Investigations of the atomic structure of minerals published in *America Mineralogist* use techniques of X-ray diffraction and transmission electron microscopy to locate the positions of oxygen atoms in relation to other chemical elements composing a crystal. That oxygen dominates the volume in minerals is obscured, however, by the conventional representation of atomic structures by coordination polyhedra. Oxygen is consigned to the corners of polyhedra enclosing silicon, aluminum, iron and other elements. The volume occupied by each oxygen atom in relation to its nearest neighbors in a crystal structure is difficult to visualize in the mind's eye from textbook representations. Oxygen is visible as "bumps" in electron density maps made in the analysis of the atomic structure of minerals with X-ray diffraction, but, because of its lower capacity to scatter X-rays, oxygen does not appear to fill space to the same extent as implied by its atomic radius in coordination polyhedra. Do mineralogical studies inadvertently downplay the importance of oxygen? Has oxygen been relegated to a supporting role as a bit-player merely serving to maintain electrical neutrality and minimize mutual repulsion between cations in minerals? Acknowledging decades of success by mineralogists in seeking to understand atomic structures in minerals, is there

more to be learned about minerals' formation processes from oxygen? In what follows, I would like to celebrate the central significance of oxygen's third isotope in understanding Earth.

The third isotope of oxygen, ^{17}O, is quite rare in rocks and minerals, amounting to barely 0.04% of total oxygen with the balance made up by ^{16}O, 99.75% and ^{18}O, 0.21%. The third isotope of oxygen was ignored for decades by stable isotope geochemists because it was thought to trail behind the more abundant ^{18}O with values of $\delta^{17}O$ approximately 1/2 that of measured $\delta^{18}O$ owing to the dependence of isotopic fractionation on mass differences. According to this view, nothing could be learned from measuring $^{17}O/^{16}O$ that could not be discovered by measuring the more abundant $^{18}O/^{16}O$. There was little interest in measuring $^{17}O/^{16}O$ until the discovery of non-mass dependent fractionations in meteorites (Clayton et al. 1973). Elements with three or more stable isotopes, like oxygen's ^{16}O, ^{17}O, and ^{18}O, afford deeper insights into Earth's origin and evolution because measurement of two, or more, isotope ratios of an element illuminates the contrasting controls of reaction-specific fractionation vs. initial composition. Measuring multiple isotope ratios of a multi-isotope element requires patience, care, and a rigorous technique. The single-substituted isotopologue, $^{16}O^{17}O$, is 10^{-4} less abundant than the predominant $^{16}O^{16}O$ yet measurements are made routinely with a precision in $\delta^{17}O$ of 0.1 ‰, or better. Measurement of $^{17}O/^{16}O$ and $^{18}O/^{16}O$ in minerals requires high mass-resolution ion microprobes or specialized mass spectrometers with the use of hazardous chemicals such as fluorine in sample preparation: little more than a dozen labs

around the globe are currently active in analysis. Despite these difficulties, the third isotope is crucially decisive in geochemical, atmospheric, and cosmochemical research.

The measurement of elements with two stable isotopes in Earth studies is widely applied. Ratios of D/H record rainfall from the equator to poles. Variations in $^{13}C/^{12}C$ distinguish inorganically precipitated from photosynthetic carbon. Nitrogen isotope ratios, $^{15}N/^{14}N$, trace food consumption from plants to grazers to predators. Insights gained from these isotopes are unquestionably significant but their analysis inevitably offers a limited, "one-dimensional" mapping of origins vs. processes. Ambiguity in understanding arises because ranges of characteristic ratios are not unique. Different carbon fixation mechanisms in plants, for example, produce overlapping $^{13}C/^{12}C$ ratios. The meteoric water cycle can be tracked by either of the ratios D/H or $^{18}O/^{16}O$ but definitive conclusions are achieved when both sets of isotopes are measured: two "one-dimensional" discriminants gain clarity when both are used together "two-dimensionally". Measuring the abundances of the three stable oxygen isotopes and their isotopologues adds "multi-dimensionality" to geochemical investigations.

Doubly substituted molecules such as $^{17}O^{18}O$ are even less abundant than single-substituted ones, only 10^{-6} relative to $^{16}O^{16}O$. While more difficult to analyze, measurement of two "clumped" oxygen isotopologue ratios such as $^{17}O^{18}O/^{16}O^{16}O$ and $^{18}O^{18}O/^{16}O^{16}O$ leads to understanding the competition between equilibrium isotopic exchange vs. irreversible kinetic isotope fractionation. Equilibrium isotope exchange is driven by small differences in zero point energies between doubly-substituted molecules

(Eiler and Schauble, 2004). Kinetic isotope fractionations arise from a variety of causes: of current interest are isotope fractionations controlled by the atomic topography of catalytic enzymes secreted by living organisms.

The determinative role played by ^{17}O in understanding Earth will be illustrated in this review by discussing two examples, one involving the singly-substituted isotopologues $^{17}O^{16}O$ and $^{18}O^{16}O$ the other concerning the doubly-substituted isotopologues $^{17}O^{18}O$ and $^{18}O^{18}O$. The first example traces $^{17}O^{16}O$ and $^{18}O^{16}O$ back in time for 4.3 billion years to a molten globe recovering from the shock of a giant impact. The second example considers the distinctive behaviors of $^{17}O^{18}O$ and $^{18}O^{18}O$ during photosynthesis as it is occurring presently.

The Third Isotope And Early Earth History

Earth's record of O-isotope fractionation has remained remarkably the same over the entirety of its geological history. Ocean island basalts (OIB) less than 1 million years in age overlap the $\delta^{17}O$ and $\delta^{18}O$ values of a detrital zircon crystal 4,374 (+/- 6) million years old (Fig. 1; Valley et al. 2014; Starkey et al. 2016). Analyses of some 650 rocks and minerals define a linear trend passing through the compositions of the OIB's and the Hadean zircon (Fig. 1). Values of $\delta^{18}O$ vary over 24 ‰, those of $\delta^{17}O$ over 12 ‰ encompassing the known ranges for analyzed igneous and metamorphic rocks. The samples are representative of isotope fractionation effects taking place between multiple minerals or between minerals and magmas over temperatures of approximately 400 to

This is a preprint, the final version is subject to change, of the American Mineralogist (MSA)
Cite as Authors (Year) Title. American Mineralogist, in press.
DOI: http://dx.doi.org/10.2138/am-2018-6137

1200 °C. To fully appreciate the data plotted in Fig. 1 it is worth asking: Are there other geochemical parameters maintaining such invariant behavior over 4 billion years? How is such a consistent behavior achieved?

To answer these questions I turn to a comparison of the behavior of oxygen and other light elements with three or more stable isotopes. The elements O, Mg, Si, make up important rock-forming silicate minerals in Earth's crust and mantle. Sulfur is the essential ingredient of ore-bearing sulfide minerals. Isotopes of the light elements O, Mg, Si, and S are more strongly fractionated by processes such as magmatic differentiation or weathering than elements of higher atomic weight. The magnitude of isotopic fractionation for these elements depends not only on mass differences between isotopes but also on the mineral structures into which they are substituted as well as temperature (Schauble 2004). Numerous studies seek to correlate their fractionation patterns with specific chemical and mechanical processes thus providing much data for comparisons.

Sulfur

Sulfur consists of the stable isotopes ^{32}S (94.93%), ^{33}S (0.76 %), ^{34}S (4.29 %), and ^{36}S (0.02%). Hulston and Thode (1965) sought evidence to distinguish stellar nucleosynthetic effects from terrestrial chemical processes by analyzing sulfur isotopes in meteorites and terrestrial samples. They predicted that injections of isotopically heterogeneous material of stellar origin into the solar nebula would introduce offset trends or mixing lines distinct from the pattern of Fig. 1. If linear plots of $\delta^{34}S$ vs $\delta^{33}S$ and of $\delta^{34}S$ vs $\delta^{36}S$ were found, however, resembling the linear trend of Fig. 1, this would

indicate equilibrium and kinetic fractionation effects taking place during terrestrial chemical processes such as magmatic differentiation and crystallization. Analyses of both terrestrial and meteorite samples fell on the same trend with $\delta^{34}S$ (x-axis) vs $\delta^{33}S$ showing a slope of approximately 0.5 and $\delta^{34}S$ (x-axis) vs $\delta^{36}S$ a slope of 1.9. These are the effects predicted theoretically for equilibrium or kinetic isotope fractionation during chemical reactions as the slopes correspond to the mass differences $(^{33}S - {}^{32}S)/(^{34}S - {}^{32}S) = 1/2$ and $(^{36}S - {}^{32}S)/(^{34}S - {}^{32}S) = 2$. Linear trends in co-varying isotope ratios such as those of Fig. 1 are, accordingly, termed mass-dependent fractionation (see reviews: Bao et al. 2016; Dauphas and Schauble, 2016). Mass-independent (or non-mass dependent) fractionation data in plots of $\delta^{34}S$ vs $\delta^{33}S$ would define trends independent of the mass differences between isotopes. Hulston and Thode concluded that there was no evidence of sulfur isotope heterogeneities in solar system samples due to stellar nucleosythesis. With improvements in analytical techniques since the work of Hulston and Thode, meteorites are now know to have anomalies in $\Delta^{33}S$ ranging over 0.25‰ (where $\Delta^{33}S = \delta^{33}S\text{-}1000((\delta^{34}S /1000 + 1)^{0.515} -1)$, Labidi et al. 2017).

Subsequent research on terrestrial Archean rocks and minerals found large departures from the mass-dependent trends of Hulston and Thode (1965). Farquhar et al. (2000) analyzed sedimentary samples 2.5 billion years or older discovering both positive and negative deviations in ^{33}S and ^{36}S spanning some 10‰ in $\Delta^{33}S$ ($\Delta^{33}S = \delta^{33}S - 1000((\delta^{34}S /1000 + 1)^{0.515} - 1)$. Mass-independent fractionation of sulfur isotopes in ancient rocks is caused by photolysis of volcanic SO_2 by solar UV photons. If oxygen had been present in the Archean atmosphere, the formation of ozone would have shielded SO_2

This is a preprint, the final version is subject to change, of the American Mineralogist (MSA)
Cite as Authors (Year) Title. American Mineralogist, in press.
DOI: http://dx.doi.org/10.2138/am-2018-6137

161 from photolysis. Mass-independent fractionation of sulfur isotopes demonstrates the
162 presence of an oxygen-free atmosphere.

163 ***Magnesium***

164 Magnesium stable isotopes, ^{24}Mg (79%), ^{25}Mg (10%), and ^{26}Mg (11%), measured
165 in terrestrial samples resemble the behavior of oxygen isotopes. Values of δ^{26}Mg (x-axis)
166 plotted vs. δ^{25}Mg lie along a linear trend with a slope of approximately 1/2, given by the
167 ratio of mass differences (^{25}Mg - ^{24}Mg) / (^{26}Mg - ^{24}Mg) (see review Teng, 2017).
168 Magnesium isotopes in primitive meteorites do not follow a mass dependent trend,
169 however. The short-lived radioactive isotope ^{26}Al produced during supernovae and
170 injected into the solar nebula decays to ^{26}Mg with a half-life of 7 X 10^5 years. The decay
171 of ^{26}Al leaves a residue of excess ^{26}Mg in meteorites dating from the earliest history of
172 the solar system provided that the ancient stones have not been processed by subsequent
173 planetary events (see review Young and Galy, 2004).
174

175 ***Silicon***

176 Silicon has three stable isotopes, ^{28}Si (92.2%), ^{29}Si (4.7%), and ^{30}Si (3.1%). Plots
177 of δ^{30}Si (x-axis) vs. δ^{29}Si analytical data for terrestrial samples define a linear array with
178 slope approximately = 1/2 (see review, Poitrasson 2017). Analyses of both chondritic and
179 achondritic meteorites show no deviations from the mass dependent linear fractionation
180 trend of terrestrial samples (Pringle et al. 2013).
181
182

183 **Oxygen**

Given the univariant behavior of oxygen isotope data in Fig. 1, it is not surprising that early geochemical research focused on measuring $\delta^{18}O$, alone. If $\delta^{17}O$ values follow the mass-dependent rule of Fig. 1, there is no need to measure the variable because its value can be calculated from an analysis for $\delta^{18}O$, ie $\delta^{17}O = 0.52* \delta^{18}O$ (approximately). Neglecting $\delta^{17}O$ analysis became untenable, however, when large deviations in oxygen isotope compositions from the plot of fig. 1 were found in meteorites (Clayton et al. 1973). The linear trend of terrestrial rocks and minerals shown in Fig. 1 was recognized at this time and adopted as the "TFL", the terrestrial fractionation line, to serve as a benchmark for reporting meteorite anomalies. The metric $\Delta^{17}O = 0.52*\delta^{17}O - \delta^{18}O$ was chosen for reporting deviations from the TFL. Positive values of $\Delta^{17}O$ identify samples plotting above the TFL, negative values those plotting below the TFL. Subsequent systematic surveys of meteorite samples found different petrographic classes of meteorites to plot along linear arrays as in Fig. 1 but offset from one another (Clayton and Mayeda, 1983). The eucrites, now associated with the asteroid 4 Vesta (Drake 1981), with negative $\Delta^{17}O$, traced a mass dependent trend 0.3 ‰ below the TFL (Figure 2B). Triple oxygen isotope analyses of shergottite, nakhlite, and chassignite meteorites, now known to have Mars as their parent body (Bogard et al. 1984), plotted 0.3 ‰ above the TFL. It was suggested by Clayton and Mayeda (1983) that each of the groups of meteorites whose $\delta^{18}O$ and $\delta^{17}O$ values plot on a mass-dependent fractionation line originated on separate planetary bodies and underwent magmatic differentiation on those bodies before being hurled into earth-crossing orbits by impacting meteorites. As many as 110 separate parent bodies are now known based on O-isotope analyses of meteorites

(Greenwood et al. 2016). Oxygen isotopes in primitive meteorites unprocessed by planetary chemistry and in the solar wind are fractionated mass independently with plots of $\delta^{18}O$ vs $\delta^{17}O$ lying on a linear trend with slope of 1. The O-isotope heterogeneity of the solar system ranges over 250 ‰ in $\delta^{18}O$ and 100 ‰ in $\Delta^{17}O$ (McKeegan et al. 2011; Sakamoto et al. 2007). Oxygen's isotopic heterogeneity predates the oldest solid objects in the solar system, the calcium-aluminum inclusions of primitive meteorites. Mass independent fractionation in the solar nebula was caused by ultra-violet photodissociation of CO molecules in molecular clouds during ignition of the Sun (Lyons and Young, 2005).

Mass-independent oxygen isotope anomalies are produced on Earth when atmospheric oxygen is photolyzed by solar UV photons. The resulting ozone is anomalously enriched in both ^{17}O and ^{18}O relative to ^{16}O (Mauersberger et al. 2003; Thiemens 2006). Apart from its role in shielding Earth from UV radiation, ozone's isotopic anomalies are valued as tracers of interactions between the atmosphere and Earth's surface mineralogy. The ^{17}O and ^{18}O enrichments in ozone are transferred to sulfate, nitrate, and perchlorate anions by atmospheric reactions. These anomalies accumulate in aerosols, falling to the surface, where they react with wind-blown sea salt or calcite dust. The minerals so formed, anhydrite, $CaSO_4$, or soda niter, $NaNO_3$, are water soluble but persist in arid desert regions. The $\Delta^{17}O$ anomalies of these minerals are positive and range over ten's of per mil (Bao et al. 2000; Michalski et al. 2003). The atmospheric anomalies, although large in magnitude, do not effect Earth's bulk crust and mantle composition because they are ephemeral and easily diluted by rainfall.

This is a preprint, the final version is subject to change, of the American Mineralogist (MSA)
Cite as Authors (Year) Title. American Mineralogist, in press.
DOI: http://dx.doi.org/10.2138/am-2018-6137

Comparison of O-, S-, Mg- and Si-isotopes

Oxygen shares a characteristic feature with other rock-forming elements having 3 or more isotopes: mass dependent fractionation. The isotopes of O, S, Mg, and Si in terrestrial rocks and minerals plot on linear trends following the predictions of Huston and Thode (1965) for isotope fractionation during equilibrium or kinetically controlled chemical processes such as magmatic differentiation, metamorphism, diagenesis, surface weathering, or the metabolism of living organisms. Oxygen and sulfur isotopes share a vulnerability to mass independent fractionation in Earth's atmosphere by reactions induced by solar UV photolysis (Bao et al. 2000; Farquhar et al. 2000). Magnesium isotopes in primitive meteorites show small enrichments in ^{26}Mg owing to the decay of short-lived radioactive ^{26}Al in the very early history of the solar system. The reservoirs sequestering these anomalies are of limited extent relative to Earth's crust and mantle.

Now let me return to Fig. 1 for it is the 4 billion-year-old terrestrial fractionation of oxygen isotopes that remains the focus of the present discussion. The foregoing comparisons demonstrate the prevalence of mass dependent fractionation in rock-forming elements that have three or more elements, at least in those that are not vulnerable to UV photodissociation. Planetary processes such as magmatic differentiation and crystallization are effective in driving isotope distributions towards equilibrium, mass dependent fractionations. Oxygen stands apart from S, Mg, and Si, however in the large range in its isotopic heterogeneity in the solar system. The solar system was homogeneous in Mg, Si and S isotopes prior to planetary accretion. It was heterogeneous

252 in oxygen isotopes. If Earth were built up of accreting planetesimals with as wide a
253 heterogeneity in O-isotopes as is presently measured in meteorites and if there had been
254 no mixing process to homogenize the aggregate, a single linear trend as in Fig. 1 would
255 not be observed. In its place, a plot of $\delta^{18}O$ vs. $\delta^{17}O$ would show a myriad of mutually
256 parallel mass dependent fractionation lines each recording localized isotopic equilibration
257 or domains failing to equilibrate retaining the primordial slope 1 line of the nebula. Fig.
258 2a,b shows what Earth might have looked like at an early stage in its history, prior to
259 homogenization.
260
261 The meteorite NWA 5232 records both early global melting on the eucrite parent
262 body but also subsequent disruption by colliding carbonaceous chondrites. The meteorite
263 consists of gray eucrite fragments decorated with exotic, angular clasts of black CM
264 carbonaceous chondrites (Fig. 2A; van Drongelen et al. 2016). The black clasts are easily
265 visible, up to several millimeters in diameter, and embedded in a groundmass of
266 brecciated eucrite (Fig. 2A). The oxygen isotopic compositions of the CM chondrite
267 clasts lie far below the TFL and scatter along a trend with a slope of approximately 1.0 on
268 a $\delta^{18}O$ vs. $\delta^{17}O$ plot (Fig. 2B). Spot analyses of eucritic breccia fragments plot along a
269 mass dependent fractionation line with slope of approximately 0.52 located 0.26 ‰
270 below the TFL (Fig. 2B). The distinction between the O-isotope relationships of a
271 globally homogenized vs. a heterogeneous planetary body is clearly seen by comparing
272 Figs. 1 and 2. Oxygen isotope compositions of NWA 5232 do not lie along a single mass
273 dependent fractionation trend derived from a homogeneous parent body. Some 650 O-
274 isotope analyses of Earth's rocks and minerals, in contrast, define a single line as is

expected from the homogenization of a parent body by melting. Robert et al. (1992) concluded that Earth had become a well-mixed body by 3.5 billion years. Rumble et al. (2013) and Valley et al. (2014) measured mass dependent fractionation lines in Hadean and Archean rocks and argued that Earth experienced an episode of O-isotope homogenization caused by global melting prior to 4.35 billion years.

Readers should evaluate these conclusions by considering alternative views. Javoy et al (2010) have proposed that Earth was built up from parent bodies closely similar in O-isotopes to the present terrestrial composition. If their hypothesis is correct, no homogenization is required. Dauphas (2017) reviewed evidence for the accretion of Earth from enstatite chondrites and aubrites. Fitoussi et al. (2016) considered Earth to have been assembled from a mixture of meteorite types including chondrites as well as differentiated achondrites. The question of proto-Earth's heterogeneity or homogeneity remains open.

The most probable cause of Earth's oxygen isotope homogenization is global melting generated by a series of impacts during accretion, prior to 4.3 billion years. A giant, Moon-forming impact would have provided ample energy to melt both proto-Earth and its impactor (Cuk and Stewart, 2012; Canup, 2012). Convection in impact-generated silicate magmas combined with simultaneous isotope exchange between liquid and impact-generated vapor would mix and homogenize oxygen isotopes in a mere 1000 years (Pahlevan and Stephenson, 2007).

This is a preprint, the final version is subject to change, of the American Mineralogist (MSA)
Cite as Authors (Year) Title. American Mineralogist, in press.
DOI: http://dx.doi.org/10.2138/am-2018-6137

The third isotope of oxygen, ^{17}O, long recognized by cosmochemists as an indispensible means of distinguishing between extraterrestrial parent bodies of meteorites, now plays an important role in understanding Earth's earliest history. The remarkable consistency of a linear trend in plots of $\delta^{18}O$ vs. $\delta^{17}O$ for Earth's rocks and minerals over most of Earth history (Fig. 1) is caused by (1) a tendency towards isotopic equilibration resulting in mass dependent fractionation; and (2) an episode of oxygen isotopic homogenization prior to 4.3 billion years. Measurements of $^{17}O/^{16}O$, from rocks ranging in age from as old as 4.3 billion years to less than 1 million years, give permissive evidence of homogenization during a Hadean magma ocean.

The Third Isotope of Oxygen and Photosynthesis

The fossilization of plants creates fascinating mineralogy with faithful preservation of the forms of leaves and cell walls. Plant fossils from Jurassic blue-schist, lawsonite-bearing rocks of New Zealand offer worthy objects of study for mineralogists as evidence of ancient photosynthesis (Galvez et al. 2012). Fossil evidence of photosynthesis is rare, however in the ancient geological record. Deformation and metamorphism effectively erase plant fossils in older rocks.

Isotopic fossils, however, such as distinctive isotopic compositions diagnostic of photosynthesis, may afford a more durable record in ancient Earth. Biomarkers or isotopic proxies of photosynthesis must first be validated by study of modern processes before application in a search for the history of photosynthesis. Please bear in mind that

every weathered sulfide mineral, every soil horizon, every plant, shell, bone, tooth, and fleshy part of the biosphere that interacted with the atmosphere contains oxygen produced by photosynthesis. Given the distinctive isotopic signatures discussed below, each weathering rind, each fossil carries a potential record of the evolution of photosynthesis. An important challenge for mineralogists is discerning the most favorable mineralogical archives in which geological atmospheric and biological history can be read. This centennial review is written in hopes of recruiting new colleagues in the search for geological records of "soft" processes poorly recorded in Earth's history. An inspiring example of what is needed is the discovery of anomalous fractionations of the four stable isotopes of sulfur isotope in Archean sulfide and sulfate minerals demonstrating Earth's ancient, oxygen-free atmosphere, (Farquhar et al. 2000). A record of ozone produced by photolysis of oxygen by ultraviolet light was found in the non-mass dependent fractionation of three oxygen isotopes in sulfate minerals as old as the Tertiary (Bao et al. 2000). Searching the geological record for isotopic evidence of ephemeral atmospheric and biological processes, such as photosynthesis, will be amply repaid by gaining deeper insights into the history of life on Earth.

Plants produce oxygen from the water in which they grow by photosynthesis. Photosynthesis does not achieve oxygen isotope exchange equilibrium between subtstrate H_2O and O_2: The isotopic composition of photosynthetic O_2 approaches that of the H_2O from which it is derived (Guy, Fogel, & Berry, 1983). Given that mid- to high-latitude meteoric water has a negative $\delta^{18}O$, photosynthesis produces O_2 depleted in $^{16}O^{17}O$ and $^{16}O^{18}O$. Plant respiration, preferentially consuming $^{16}O^{16}O$, in contrast, enriches residual

This is a preprint, the final version is subject to change, of the American Mineralogist (MSA)
Cite as Authors (Year) Title. American Mineralogist, in press.
DOI: http://dx.doi.org/10.2138/am-2018-6137

344 O_2 in $^{16}O^{17}O$ and $^{16}O^{18}O$, reversing the photosynthetic trend. Successive measurements of
345 oxygen isotope compositions in the atmosphere of a closed terrarium experiment show
346 steady depletions in $^{18}O/^{16}O$ as long as light is available to drive photosynthesis,
347 approaching the $^{18}O/^{16}O$ of substrate water. Once the lights are turned off, however,
348 $^{18}O/^{16}O$ ratios begin to rise in terrarium O_2 as it is consumed by dark respiration. The
349 same effects are seen in $^{17}O/^{16}O$ for analyses of oxygen in closed terrariums (Fig. 3,
350 plotted from Luz & Barkan, 2005). The ramifications of these effects are profound.
351 Atmospheric O_2 is not in isotopic exchange equilibrium with seawater, a condition
352 termed the "Dole Effect", after its discoverer (Dole, 1952). The current steady state
353 composition of the atmosphere, $\delta^{18}O_{VSMOW}$ = +23‰, is a balance between the tendency
354 of photosynthesis to drag down its $^{18}O/^{16}O$ towards that of meteoric or sea water vs.
355 enrichment in $^{18}O/^{16}O$ by both plant and animal respiration (Bender et al. 1994; Luz &
356 Barkan, 2005; Young et al. 2015)
357
358 ***Double-substituted Isotopologues and Photosynthesis***
359
360 The third isotope of oxygen, ^{17}O, substitutes not only in oxygen molecules like
361 $^{16}O^{17}O$ but also in the molecules $^{17}O^{17}O$ and $^{17}O^{18}O$. The latter two molecules are termed
362 "doubly-substituted" or "clumped" because two rare, heavy isotopes are present in each.
363 The investigation of isotopically doubly-substituted molecules was pioneered by Eiler &
364 Schauble (2004) and Wang, Schauble & Eiler (2004). These authors presented original
365 data on the clumped isotopologue $^{13}C^{18}O^{16}O$ in the atmosphere. It was predicted that
366 analysis of doubly-substituted isotopologues in gases, liquids, and solids would reveal

367 distinctive fractionation patterns, both equilibrium and kinetic, with great potential for
368 understanding processes in nature such as carbonate diagenesis, diffusion, gravitational
369 settling, metabolism, and photochemistry. Their prediction has been borne out by a
370 cornucopia of fascinating research results. In this brief review, research on ^{17}O
371 substituted in $^{17}O^{18}O$ (and also $^{18}O^{18}O$, lacking in ^{17}O) will be discussed, emphasizing the
372 advantages of measuring two doubly-substituted isotopologues in the same gas species
373 (Yeung et al. 2015; 2016)
374
375 The abundances of the doubly-substituted isotopologues, $^{17}O^{18}O$ and $^{18}O^{18}O$ in O_2
376 gas, are expressed as Δ_{35} (in ‰) = $[((^{17}O^{18}O/^{16}O^{16}O)_{measured}/(^{17}O^{18}O/^{16}O^{16}O)_{stochastic})$-
377 1]*1000, and Δ_{36} (in ‰) = $[((^{18}O^{18}O/^{16}O^{16}O)_{measured}/(^{18}O^{18}O/^{16}O^{16}O)_{stochastic})$-1]*1000
378 (Yeung et al. 2012). Because $^{17}O^{17}O$ is 10 times less abundant than $^{17}O^{18}O$, and
379 correspondingly more difficult to measure, it will not be considered further. The ratios
380 $^{17}O^{18}O/^{16}O^{16}O$ (^{35}R) and $^{18}O^{18}O/^{16}O^{16}O$ (^{36}R) are measured in an unknown sample
381 relative to a calibrated O_2 reference gas as well as the single-substituted ratios
382 $^{16}O^{17}O/^{16}O^{16}O$ (^{33}R) and $^{16}O^{18}O/^{16}O^{16}O$ (^{34}R) using conventional reference-unknown-
383 reference comparison in a dual inlet, multi-collector gas source mass spectrometer.
384 Single-substituted ratios are used to estimate the bulk oxygen isotopic composition of
385 each unknown from which its stochastic isotopologue distribution is calculated. The
386 calculated stochastic ^{35}R and ^{36}R values are then used to calculate Δ_{35} and Δ_{36}. Note,
387 especially, that the $^{35}R_{stochastic}$ and $^{36}R_{stochastic}$ values refer to the unknown, not to the
388 reference gas.
389

This is a preprint, the final version is subject to change, of the American Mineralogist (MSA)
Cite as Authors (Year) Title. American Mineralogist, in press.
DOI: http://dx.doi.org/10.2138/am-2018-6137

Please consider a comparison between analytical reporting conventions for single-substituted and doubly-substituted isotopologues. For $^{16}O^{17}O/^{16}O^{16}O$ and $^{16}O^{18}O/^{16}O^{16}O$, data are reported as $\delta^{17}O_{VSMOW}$ and $\delta^{18}O_{VSMOW}$ in relation to the composition of an internationally recognized calibration of seawater, "VSMOW ", ie "Vienna Standard Mean Ocean Water". For $\Delta^{17}O$, analytical data is reported in relation to the Terrestrial Fractionation Line, TFL (Fig. 1). The calibrated reference is distinct from the unknown under investigation. Doubly-substituted isotopologues Δ_{35} and Δ_{36}, however, are reported in relation to a self-referencing calibration, the stochastic distribution calculated uniquely for each bulk ^{16}O-^{17}O-^{18}O composition of O_2. It is well to keep in mind that a quantitative enumeration of the distribution of isotopologues in a specific gas is necessarily self-referencing because each gas isotopic bulk composition has its own unique stochastic distribution. While the use of a calculated stochastic reference unique for each unknown sample as a benchmark for isotopic enrichments and depletions may be unfamiliar, the convention is also used to describe the distribution of ^{16}O-^{17}O-^{18}O in ozone isotopologues (Mauersberger et al. 1999).

To gain deeper understanding of doubly-substituted isotopologues it is helpful to consider the ordering and disordering of stronger and weaker bonds between heavier and lighter isotopes in molecules. Readers of the *American Mineralogist* are familiar with order-disorder distributions of chemical elements on sites in crystalline phases. Cation exchange reactions between sites within minerals are analogous to isotope exchange reactions between gas molecules in that they are both driven by changes in temperature without necessarily changing bulk chemical or isotopic compositions. In crystals, heating

This is a preprint, the final version is subject to change, of the American Mineralogist (MSA)
Cite as Authors (Year) Title. American Mineralogist, in press.
DOI: http://dx.doi.org/10.2138/am-2018-6137

413 to just below melting stimulates thermal vibrations of atoms and may lead to elemental
414 exchange between crystallographically defined sites. An ordered low temperature
415 distribution of atoms arranged on sites to minimize potential energy may give way to a
416 random distribution upon heating. Consider the distribution of Al and Si on the
417 tetrahedral sites of potassium feldspar. High temperature sanidine found in rhyolites has a
418 randomized, stochastic distribution of Al and Si; its tetrahedral sites are indistinguishable
419 chemically from one another. Orthoclase from granite of lower crystallization
420 temperature, however, features non-stochastic Al/Si ratios ordered on distinct tetrahedral
421 sites (Thompson, 1969, Fig. 3, p. 359). The comparison must not be carried too far: for
422 potassium feldspar, the energy associated with ordering includes elastic contributions
423 from substituting the larger Al for Si (e.g. Carpenter 2000) as well as the avoidance of Al
424 substitution in adjacent tetrahedra (Lowenstein 1954). There are no such constraints in
425 isotope exchange reactions between gas molecules because different isotopes of the same
426 element have the same size and same configuration of electrons. The order-disorder
427 behavior of isotopes is therefore expected to follow the Bragg-Williams model (Bragg
428 and Williams, 1934) for order-disorder in alloys that only considers the energetic
429 contributions of nearest-neighbor interactions and does not include the long-range effects
430 found in minerals such as feldspars.
431
432 Order-disorder in oxygen gas is controlled by the increasing bond strength of the
433 six isotopologues, in order $^{16}O^{16}O$, $^{16}O^{17}O$, $^{16}O^{18}O$, $^{17}O^{17}O$, $^{17}O^{18}O$, and $^{18}O^{18}O$, from
434 weakest to strongest bonding. Isotopic exchange between isotopologues minimizes the
435 potential energy of the molecular aggregate. The distribution for a given bulk ^{16}O-^{17}O-

This is a preprint, the final version is subject to change, of the American Mineralogist (MSA)
Cite as Authors (Year) Title. American Mineralogist, in press.
DOI: http://dx.doi.org/10.2138/am-2018-6137

436 ^{18}O composition is determined by temperature or, in the event equilibrium is not achieved,
437 by reaction kinetics. An additional factor in determining the abundances of doubly-
438 substituted isotopologues has been found: the nature of the reservoir or reservoirs from
439 which isotopes are drawn to form molecules. Combinatorial statistics may have a strong
440 effect on isotopically-substituted molecules (Yeung et al. 2015; Yeung 2016; Rockmann
441 et al. 2016). An example of combinatorial effects in photosynthetic O_2 is given below.
442
443 A calculated equilibrium curve for Δ_{35} vs. Δ_{36} in O_2 gas, contoured in °C, shows
444 Δ_i values decreasing with increasing temperature to a value of zero, fully stochastic, at
445 1000 °C (Fig. 4, heavy black line with T °C labels; after Wang et al. 2004). The
446 temperature dependence comes about because the ordered distribution of doubly-
447 substituted molecule at low temperature achieved by substituting heavier isotopes is
448 gradually overtaken by thermal agitation as O_2 gas is heated. Values of Δ_{35} and Δ_{36} are
449 independent of pressure because the molecular volumes of the oxygen isotopologues are
450 closely similar. Gases of any bulk composition in $\delta^{17}O$ and $\delta^{18}O$ follow the same curve
451 because the stochastic reference frame is always calculated in respect to the bulk
452 composition of each gas sample. Every unknown gas is referred to itself, to its own
453 stochastic isotopologue distribution, when calculating Δ_{35} and Δ_{36}. The quantities Δ_{35} and
454 Δ_{36} are thus quite advantageous in their potential for gas phase thermometry: they are
455 "universally" applicable to all O_2 samples provided the bulk $^{17}O/^{16}O$ and $^{18}O/^{16}O$ ratios of
456 a gas sample remain unchanged throughout the sample's thermal history. This same
457 advantage, however gives rise to a vulnerability in that any process that changes the bulk
458 composition of a gas, with or without changing the number and distribution of its

459 clumped isotopologues, will change the calculated stochastic distribution and,
460 consequently, change Δ_{35} or Δ_{36}. Consider the mixing at room temperature of two O_2
461 gases differing in bulk composition and having equilibrated at different temperatures.
462 Isotope exchange reactions are sluggish at room temperature so mixing the two gases
463 produces a gas with the same number and distribution of clumped isotopologues, but with
464 a different bulk composition. The sample's calculated values of $^{35}R_{stochastic}$ and
465 $^{36}R_{stochastic}$ will be changed and Δ_{35} and Δ_{36} will be altered. The resulting mixture will no
466 longer provide accurate geothermometry as signaled by its failure to plot on the
467 equilibrium curve of Fig. 4 (cf. Young et al. 2016, Fig. 12, p. 9).
468
469 The geothermometric potential of measuring O_2 isotopologues suggests
470 applications in atmospheric chemical and physical investigations. To fully exploit these
471 research opportunities, however, requires experimental verification that isotopic
472 exchange equilibria has been achieved between O_2 isotopologues. Measuring two doubly-
473 substituted isotopologues from the same gas sample provides a two-stage verification of
474 equilibration. If one of the isotopologues were prevented from equilibrating by an
475 irreversible reaction in the experiment, then Δ_{35} and Δ_{36} would no longer plot on the
476 equilibrium curve. Laboratory investigations of isotope exchange reactions in O_2 gas
477 during electrolysis with a Tesla coil and photolysis with ultraviolet irradiation shows that
478 catalysis by $O(^3P)$ + O_2 isotope exchange tends towards equilibration at controlled
479 temperatures (Fig. 5; Yeung et al. 2016; Yeung et al. 2014; Yeung and Young 2012).
480 Analysis of atmospheric O_2 demonstrates persistent values of Δ_{36} = 1.96 +/- 0.07 ‰ and
481 Δ_{35} = 1.0 +/- 1.0 ‰ lying on the equilibrium curve (Fig. 5; Yeung et al. 2016).

This is a preprint, the final version is subject to change, of the American Mineralogist (MSA)
Cite as Authors (Year) Title. American Mineralogist, in press.
DOI: http://dx.doi.org/10.2138/am-2018-6137

482

483 Photosynthesis, in contrast to the isotope equilibrium of atmospheric reactions
484 catalyzed by $O(^3P) + O_2$, does not achieve isotopic equilibrium, neither in single-
485 substituted nor in doubly-substituted isotopologues (compare Fig. 5; Fig. 6). Oxygen
486 produced by photosynthesis in the light departs increasingly from equilibrium
487 distributions of $^{17}O^{18}O$ and $^{18}O^{18}O$. Over the course of a year's time, abundances of
488 doubly-substituted molecules decrease continually towards stochastic values, in some
489 cases reaching negative, "anti-clumping", values (Fig. 6). In contrast, abundances of
490 $^{17}O^{18}O$ and $^{18}O^{18}O$ in residual O_2 increase during plant respiration, returning towards
491 equilibrium, in a dark, closed terrarium.

492

493 Please take a second look at Figure 6. That a closed photosynthetic system
494 operating at room temperature produces oxygen with Δ_{35} and Δ_{36} distributions surpassing
495 those of equilibrium at 1000 °C is quite surprising. How is such an anomalous result to be
496 explained? It is known that plants take up substrate water, split two H_2O molecules to
497 obtain $4H^+$ for their metabolism, and discard unwanted oxygen as O_2. The protein
498 Photosystem II is responsible for converting H_2O to hydrogen ions and O_2. Suppose the
499 two waters split by Photosystem II do not have equal $^{18}O/^{16}O$ and $^{17}O/^{16}O$. The
500 combinatorial formulas used in calculating stochastic distributions customarily assume
501 that ^{16}O, ^{17}O, and ^{18}O isotopes are drawn randomly from a homogeneous reservoir of
502 oxygen isotopes. Yeung et al. (2015) realized, however, that drawing isotopes randomly
503 from two reservoirs, that is, two H_2O sites, differing in $^{17}O/^{16}O$ and $^{18}O/^{16}O$, requires a
504 different combinatorial formula. Using a corrected formula gives negative values for Δ_{35}

This is a preprint, the final version is subject to change, of the American Mineralogist (MSA)
Cite as Authors (Year) Title. American Mineralogist, in press.
DOI: http://dx.doi.org/10.2138/am-2018-6137

and Δ_{36} like those measured: Δ_{36} (photosynthesis) = $\{[\alpha_A\alpha_B/0.25(\alpha_A+\alpha_B)^2]-1\}$, where α_A and α_B denote two separate water reservoirs, A and B with $\alpha_A = [(^{18}O/^{16}O_{\text{bound water}})/(^{18}O/^{16}O_{\text{substrate water}})]$ not equal to α_B (Yeung 2016; Roeckmann et al. 2016).

The results on photosynthesis are important because they suggest the atomic structure of Photosystem II, the enzyme responsible for O_2 production, may directly control the isotopic composition of photosynthetic oxygen. The two water sites may only have different $^{18}O/^{16}O$ if their atomic coordination environments are different. If all the water molecules are coordinated to identical atomic nearest neighbors there would be no energetic advantage in substituting more or less ^{18}O. If, however, waters are coordinated differently, it would be possible, in principle, to stabilize Photosystem II by substituting different $^{18}O/^{16}O$ in H_2O sites (Fig. 7). Femtosecond x-ray diffraction of the oxygen evolving complex (OEC) embedded in Photosystem II shows four H_2O molecules, two (W1 & W2) coordinated to Mn (Mn4A) and two (W3 & W4) coordinated to Ca atoms (Fig.7; Suga et al. 2015 Fig. 1d, p. 100). Each pair of H_2O sites is coordinated to different cations, Ca and Mn. The coordination of pairs of H_2O molecules to different cations satisfies the requirement for each pair to have different $^{18}O/^{16}O$. The hypothesis of Yeung et al. (2015) on the existence of at least two different H_2O reservoirs in Photosystem II is thus confirmed.

I dare say that I'm not the only person to be shocked at the precise and delicate control exerted by atom scale enzymatic catalysis on the doubly-substituted isotope distributions of O_2 produced by photosynthesis. The OEC, a miniscule but powerful

This is a preprint, the final version is subject to change, of the American Mineralogist (MSA)
Cite as Authors (Year) Title. American Mineralogist, in press.
DOI: http://dx.doi.org/10.2138/am-2018-6137

cluster of 5 cations, 5 oxygens and 4 waters is embedded in a protein weighing in at 7 kilodaltons! And consider this: if only one of the two isotopologues, $^{18}O^{18}O$ or $^{17}O^{18}O$, had been measured, the correspondence between atomic structure and isotope effects would not have been established definitively.

In Defense of the Determination of Molecular & Crystal Structures in Understanding Isotope Fractionations

The first paragraph of this review was written to pique the interest of readers of the *American Mineralogist*, if not to provoke them. There, crystal structural analysis of oxygen in minerals was discounted to shift attention to the third isotope of oxygen. But, if you have read this far, you will be gratified to have learned that determining the positions of oxygen atoms in molecular structures plays a definitive role in understanding the mechanisms of the photosynthetic production of oxygen with its irreversible isotope fractionation effects described above.

The Value of the Third Isotope of Oxygen

Oxygen-17, the third isotope of the third element, more than repays in information gained the effort expended in its measurement. Measurement of the ratios $^{17}O/^{16}O$ and $^{18}O/^{16}O$ distinguishes initial compositions from fractionation effects, revealing mass-dependent fractionation. Analyses of $\delta^{17}O$ and $\delta^{18}O$ in rocks spanning almost the entire history of Earth reveal that the silicate portion of the crust and accessible mantle were

This is a preprint, the final version is subject to change, of the American Mineralogist (MSA)
Cite as Authors (Year) Title. American Mineralogist, in press.
DOI: http://dx.doi.org/10.2138/am-2018-6137

551 derived from a reservoir that was homogeneous in its oxygen isotope composition prior
552 to 4.3 Ga.
553
554 The measurement of clumped isotopologues provides additional parameters useful
555 in understanding isotopic exchange equilibrium, reaction mechanisms, and kinetics. The
556 third isotope, ^{17}O, plays an essential role in providing a measurable clumped molecule,
557 $^{17}O^{18}O$, to accompany analysis for the more abundant $^{18}O^{18}O$. It is quite important to
558 recognize that measuring two (or more) clumped isotopologues in the same gas species
559 serves two purposes: (1) Data on two isotopologues furnishes a criterion for validating
560 estimates of temperature of formation of gas samples by direct observation of whether or
561 not isotope exchange equilibrium is achieved. (2) The same data provide an isotopic
562 fingerprint of the kinetic isotope effects expressed during the operation of irreversible
563 reactions or processes.
564
565 **Future Perspectives**
566
567 Structural analysis of minerals by x-ray diffraction is a notable triumph for the
568 mineralogical community. Our cousins in the structural biology community are
569 crystallizing proteins to achieve diffraction with femtosecond bursts of X-rays from free
570 electron lasers too brief to destroy delicate organic crystals. Isotope geochemists for the
571 first time are able to measure the subtle effects recorded by doubly-substituted
572 isotopologues. It may seem improbable that these subtle effects are archived over
573 geological time. I would like to encourage a partnership in the search for durable isotopic

574 fingerprints of atmospheric and biological processes poorly preserved in the geologic
575 record. Mineralogists and petrologists, isotope geochemists, biogeochemists, structural
576 biologists and biochemists, all have talents needed to understand the geological history of
577 photosynthesis.
578
579 **Acknowledgements**
580
581 I would like to thank George Cody, Acting Director of the Geophysical
582 Laboratory, for support in writing this article. Jesse Ausebel, Robert Hazen and Craig
583 Schiffries of the Deep Carbon Observatory, David Lambert (NSF), Nick Woodward
584 (DOE), and J. A. Rudnick (UCLA) provided critical funding for building Panorama, a
585 high-resolution mass spectrometer for the measurement of clumped isotopologues. P. A.
586 Freedman, M. Mills, D. Rousell, and P. Li, Nu Instruments Ltd., designed, built, installed,
587 and support Panorama. I am especially grateful to Weifu Guo, WHOI, who gave
588 excellent lessons in clumped isotope geochemistry during his post-doctoral tenure at the
589 Geophysical Laboratory. Colleagues Xiahong Feng and Mukul Sharma in the Department
590 of Earth Sciences, Dartmouth College, provided excellent discussions and exceptional
591 facilities for the writing of this article. R. J. Angel provided essential advice on
592 comparing bond ordering in gas molecules to cation ordering in aluminosilicate minerals.
593 Thanks to John B. Brady, John M. Ferry, Weifu Guo, and Dan Hummer who reviewed
594 the article informally. The text was improved by the editorial comments of J. Farquhar
595 and F. Zhen.
596

References

Bao, H., Thiemens, M., Farquhar, J., Campbell, D., Lee, C., Heine, K., and Loope, D. (2000) Anomalous 17O compositions in massive sulphate deposits on the Earth, Nature, 406, 176-178.

Bao, H., Cao, X., and Hayles, J. A. (2016) Triple Oxygen Isotopes: Fundamental Relationships and Applications, Annual Reviews Earth Planetary Science, 44, 463-492.

Bender, M., Aowers, T., and Labeyrie, L. (1994) The Dole effect and its variations during the last 130,000 years as measured in the Vostok ice core: Global Biogeochemical Cycles, 8, 363-376.

Bogard, D., Nyquist, L. E., and Johnson, P. (1984) Noble gas contents of shergottites and implications for the Martian origin of SNC meteorites, Geochimica Cosmochimica Acta, 48, 1723-1739.

Bragg, W. L., and Williams, E. J. (1934) The effect of thermal agitation on atomic arrangement in alloys., Proceedings of the Royal Society of London. Series A, 145, 699-730.

Canup, R. M. (2012) Forming a Moon with an Earth-like Composition via a Giant Impact, Science, 338, 1052-1055.

Carpenter, M. (2000) Strain and elasticity at structural phase transitions in minerals: Reviews in Mineralogy and Geochemistry, 39, 35-64.

Clayton, R., Grossman, L., and Mayeda, T. (1973) A component of primitive nuclear

620 composition in carbonaceous meteorites, Science, 182, 485-488.
621 Clayton, R., and Mayeda, T. (1983) Oxygen isotopes in eucrites, shergottites, nakhlites,
622 and chassignites: Earth and Planetary Science Letters, 62, 1-6.
623 Cuk, M., and Stewart, S. T. (2012) Making the Moon from a Fast-Spinning Earth: A
624 Giant Impact Followed by Resonant Despinning, Science, 338, 1047-1052.
625 Dauphas, N., and Schauble, E. A. (2016) Mass Fractionation Laws, Mass-Independent
626 Effects, and Isotopic Anomalies, Annual Reviews Earth Planetary Science, 44,
627 709-783.
628 Dauphas, N. (2017) The isotopic nature of the Earth's accreting material through time,
629 Nature, 541, 521-524.
630 Dole, M. (1952) The Chemistry of the Isotopes of Oxygen, Chemical Reviews, 51, 263-
631 300.
632 Drake, M. J. (2001) The eucrite/Vesta story, Meteoritics and Planetary Science, 36, 501-
633 513.
634 Eiler, J., and Schauble, E. (2004) (OCO)-O-18-C-13-O-16 in Earth's atmosphere:
635 Geochimica et Cosmochimica Acta, 68, 4767-4777.
636 Farquhar, J., Bao, H., and Thiemens, M. (2000) Atmospheric Influence of Earth's Earliest
637 Sulfur Cycle Science, 289, 756-758.
638 Fitoussi, C., Bourdon, B., and Wang, X., 2016, The building blocks of Earth and Mars: A
639 close genetic link, Earth and Planetary Science Letters, 434, 51-160.
640
641 Galvez, M. E., Beyssac, O., Benzerara, K., Bernard, S., Menguy, N., Cox, S. C., Martinez,
642 I., Johnston, M. R., and Brown, G. E. (2012) Morphological preservation of

643 carbonaceous plant fossils in blueschist metamorphic rocks from New Zealand,
644 Geobiology, 10, 118-129.
645 Greenwood, R., Franchi, I., Jambon, A., and Buchanan, P. (2005) Widespread magma
646 oceans on asteroidal bodies in the early Solar System: Nature, 435, 916-918.
647 Greenwood, R. C., Burbine, T. H., Miller, M. F., and Franchi, I. A. (2017) Melting and
648 differentiation of early-formed asteroids: The perspective from high precision
649 oxygen isotope studies, Chemie der Erde - Geochemistry, 77, 1-43.
650 Guy, R., Fogel, M., and Berry, J. (1993) Photosynthetic fractionation of the stable
651 isotopes of oxygen and carbon: Plant Physiology, 101, 37-47.
652 Hulston, J., and Thode, H. (1965) Variations in the S33, S34, and S36 contents of
653 meteorites and their relation to chemical and nuclear effects, Journal of
654 Geophysical Research, 70, 3475-3484.
655 Javoy, M., Kaminski, E., Guyot, F., Andrault, D., Sanloup, C., Moreira, M., Labrosse, S.,
656 Jambon, A., Agrinier, P., Davaille, A., and Jaupart, C. (2010) The chemical
657 composition of the Earth: Enstatite chondrite models, Earth and Planetary Science
658 Letters, 293, 259-268.
659 Labidi, J., Farquhar, J., Alexander, C. M. O. D., Eldridge, D. L., and Oduro, H. (2017)
660 Mass independent sulfur isotope signatures in CMs: Implications for sulfur
661 chemistry in the early solar system, Geochimica et Cosmochimica Acta, 196, 326-
662 350.
663 Lowenstein, W. (1954) The distribution of aluminum in the tetrahedra of silicates and
664 aluminates: American Mineralogist, 39, 92-96.
665 Luz, B., and Barkan, E. (2005) The isotopic ratios O-17/O-16 and O-18/O-16 in

molecular oxygen and their significance in biogeochemistry: Geochimica et Cosmochimica Acta, 69, 1099-1110.

Lyons, J., and Young, E. (2005) CO self-shielding as the origin of oxygen isotope anomalies in the early solar nebula: Nature, 435, 317-320.

Masago, H., Rumble, D., Ernst, W., Parkinson, C., and Maruyama, S. (2003) Low delta O-18 eclogites from the Kokchetav massif, northern Kazakhstan: Journal of Metamorphic Geology, 21, 579-587.

Mauersberger, K. (1999) Ozone Isotope Enrichment: Isotopomer-Specific Rate Coefficients, Science, 283, 370-372.

Mauersberger, K., Krankowsky, D., and Janssen, C. (2003) Oxygen isotope processes and transfer reactions, Space Science Reviews, 106, 265-279.

McKeegan, K. D., Kallio, A. P. A., Heber, V. S., Jarzebinski, G., Mao, P. H., Coath, C. D., Kunihiro, T., Wiens, R. C., Nordholt, J. E., Moses, R. W., Reisenfeld, D. B., Jurewicz, A. J. G., and Burnett, D. S. (2011) The Oxygen Isotopic Composition of the Sun Inferred from Captured Solar Wind, Science, 332, 1528-1532.

Michalski, G., Scott, Z., Kabiling, M., and Thiemens, M. (2003) First measurements and modeling of Delta O-17 in atmospheric nitrate: Geophysical Research Letters, 30, 1870.

Pahlevan, K., and Stevenson, D. J. (2007) Equilibration in the aftermath of the lunar-forming giant impact: Earth and Planetary Science Letters, 262, 438-449.

Poitrasson, F. (2017) Silicon Isotope Geochemistry, Reviews in Mineralogy & Geochemistry, 82, 289-344.

Pringle, E. A., Savage, P. S., Jackson, M. G., Barrat, J.-A., and Moynier, F. (2013) Si

689 isotope homogeneity of the solar nebula, Astrophysical Journal, 779, 123-127.
690 Robert, F., Rejoumichel, A., and Javoy, M. (1992) Oxygen isotopic homogeneity of the
691 Earth - new evidence: Earth and Planetary Science Letters, 108, 1-9.
692 Rumble, D., and Yui, T. (1998) The Qinglongshan oxygen and hydrogen isotope
693 anomaly near Donghai in Jiangsu Province, China: Geochimica et Cosmochimica
694 Acta, 62, 3307-3321.
695 Rumble, D., Bowring, S., Iizuka, T., Komiya, T., Lepland, A., Rosing, M. T., and Ueno,
696 Y. (2013) The oxygen isotope composition of earth's oldest rocks and evidence of
697 a terrestrial magma ocean, Geochemistry, Geophysics, Geosystems, 14, 1929-
698 1939.
699 Sakamoto, N., Seto, Y., Itoh, S., Kuramoto, K., Fujino, K., Nagashima, K., Krot, A. N.,
700 and Yurimoto, H. (2007) Remnants of the early solar system water enriched in
701 heavy oxygen isotopes: Science, 317, 231-233.
702 Schauble, E. (2004) Applying stable isotope fractionation theory to new systems:
703 Reviews of Mineral Geochemistry, 55, 65-111.
704 Starkey, N. A., Jackson, C. R. M., Greenwood, R. C., Parman, S., Franchi, I. A., Jackson,
705 M., Fitton, J. G., Stuart, F. M., Kurz, M., and Larsen, L. M. (2016) Triple oxygen
706 isotopic composition of the high-3He/4He mantle, Geochimica et Cosmochimica
707 Acta, 176, 227-238.
708 Suga, M., Akita, F., Hirata, K., Ueno, G., Murakami, H., Nakajima, Y., Shimizu, T.,
709 Yamashita, K., Yamamoto, M., Ago, H., and Shen, J.-R. (2015) Native structure
710 of photosystem II at 1.95 Å resolution viewed by femtosecond X-ray pulses,
711 Nature, 517, 99-103.

712 Teng, F.-Z. (2017) Magnesium Isotope Geochemistry, Reviews in Mineralogy and
713 Geochemistry, 82, 219-287.
714 Thiemens, M. H. (2006) History and applications of mass-independent isotope effects,
715 Annual Reviews of Earth and Planetary Sciences, 34, 217-262.
716 Thompson jr., J. B. (1969) Chemical Reactions in Crystals, American Mineralogist, 54,
717 341-375.
718 Valley, J. W., Cavosie, A. J., Ushikubo, T., Reinhard, D. A., Lawrence, D. F., Larson, D.
719 J., Clifton, P. H., Kelly, T. F., Wilde, S. A., Moser, D. E., and Spicuzza, M. J.
720 (2014) Hadean age for a post-magma-ocean zircon confirmed by atom-probe
721 tomography, Nature Geoscience, 7, 219-223.
722 Van Drongelen, K. D., Rumble, D., and Tait, K. T. (2016) Petrology and oxygen isotopic
723 compositions of clasts in HED polymict breccia NWA 5232, Meteoritics and
724 Planetary Science, 1-17.
725 Wang, Z., Schauble, E., and Eiler, J. (2004) Equilibrium thermodynamics of multiply
726 substituted isotopologues of molecular gases: Geochimica et Cosmochimica Acta,
727 68, 4779-4797.
728 Yeung, L. Y., Young, E. D., and Schauble, E. A. (2012) Measurements of 18O18O and
729 17O18O in the atmosphere and the role of isotope-exchange reactions, Journal of
730 Geophysical Research, 117, D18306.
731 Yeung, L. Y., Ash, J. L., and Young, E. D. (2015) Biological signatures in clumped
732 isotopes of O2, Science, 348, 431-434.
733 Yeung, L. Y., Ash, J. L., and Young, E. D. (2014) Rapid photochemical equilibration of
734 isotope bond ordering in O2, Journal of Geophysical Research, 119, 10552-10566.

735 Yeung, L. Y., Murray, L. T., Ash, J. L., Young, E. D., Boering, K. A., Atlas, E. L.,
736 Schauffler, S. M., Lueb, R. A., Langenfelds, R. L., Krummel, P. B., Steele, L. P.,
737 and Eastham, S. D. (2016) Isotopic ordering in atmospheric O2 as a tracer of
738 ozone photochemistry and the tropical atmosphere, Journal of Geophysical
739 Research: Atmospheres, 121, 1-19.
740 Young, E. D., Yeung, L. Y., and Kohl, I. E. (2014) On the 17O budget of atmospheric O2,
741 Geochimica et Cosmochimica Acta, 135, 102-125.
742 Young, E., and Galy, A., (2004) The isotope geochemistry and cosmochemistry of
743 magnesium: Reviews of Mineralogy and Geochemistry, 55, 197-230.
744 Young, E., Galy, A., and Nagahara, H. (2002) Kinetic and equilibrium mass-dependent
745 isotope fractionation laws in nature and their geochemical and cosmochemical
746 significance: Geochimica et Cosmochimica Acta, 66, 1095-1104.
747 Young, E., Rumble, D., Freedman, P., and Mills, M. (2016) A large-radius high-mass-
748 resolution multiple-collector isotope ratio mass spectrometer for analysis of rare
749 isotopologues of O2, N2, CH4 and other gases, International Journal of Mass
750 Spectrometry, 401, 1-10.
751
752
753
754
755

This is a preprint, the final version is subject to change, of the American Mineralogist (MSA)
Cite as Authors (Year) Title. American Mineralogist, in press.
DOI: http://dx.doi.org/10.2138/am-2018-6137

Figure Captions

Figure 1: Plot of $\delta^{18}O$ vs. $\delta^{17}O$ showing Terrestrial Mass Fractionation Line (TFL) with VSMOW as reference. The $\delta^{18}O$ vs. $\delta^{17}O$ values of planetary bodies such as Mars and 4 Vesta lie on mass fractionation lines parallel to the TFL but offset above it (Mars) or below (4 Vesta, see Figure 2B). Data: [1]Rumble & Yui, 1998; [2]Masago et al. 2003; [3]Rumble et al. 2013; [4]Valley et al. 2014; [5]Starkey et al. 2016. Uncertainties in $\delta^{18}O$ & $\delta^{17}O$ are approximately 0.1 ‰, smaller than the plot symbols.

Figure 2: (A - left): Photograph of cut slab of meteorite NWA 5232 with $\delta^{18}O$ and $\Delta^{17}O$ values of spot analyses of CM chondrite clasts (black) and eucrite breccia fragments (gray) (van Drongelen et al. 2016). (B - right) $\delta^{18}O$ vs $\delta^{17}O$ plot of analyses of NWA 5232. The heavy black line is the TFL of Figure 1. Compare scattered distribution of data to linear array of Fig. 1. Uncertainties in $\delta^{18}O$ & $\delta^{17}O$ are approximately 0.1 ‰ and in $\Delta^{17}O$, 0.05 ‰.

Figure 3: Plot of variations in $\delta^{17}O$, $\delta^{18}O$, and $\Delta^{17}O$ vs. time in atmosphere of closed terrarium containing living *Philodendron,* soil, micro-organisns, and water. Note distinctive variations in $\delta^{17}O$ and $\delta^{18}O$ in the light and in the dark (data replotted from Luz and Barkan, 2005).

Figure 4: Plot of equilibrium curve for $\Delta^{17}O^{18}O$ (Δ_{35}) vs $\Delta^{18}O^{18}O$ (Δ_{36}) contoured in T °C (after Wang et al. 2004). The two isotopologues are assumed to coexist in isotope exchange equilibrium in the same sample of O_2 gas.

Figure 5: Plot of $\mathbf{\Delta_{35}}$ (=$\Delta^{17}O^{18}O$) vs. $\mathbf{\Delta_{36}}$ (= $\Delta^{18}O^{18}O$) for samples of O_2 gas subjected to photolysis and $O(^3P)$ + O_2 catalysis. The plotted results demonstrate a tendency towards isotope exchange equilibrium (Yeung et al. 2016). Uncertainties are 0.07‰ for $\Delta^{18}O^{18}O$ and 0.1‰ for $\Delta^{17}O^{18}O$.

Figure 6: Plot of $\Delta^{17}O^{18}O$ vs $\Delta^{18}O^{18}O$ for oxygen produced during photosynthesis in the light and residual O_2 remaining after plant respiration in the dark (Yeung et al. 2015, supplementary). The values of $\Delta^{17}O^{18}O$ vs $\Delta^{18}O^{18}O$ decrease as long as photosynthesis in the light continues. Once the light is extinguished, residual oxygen increases in $\Delta^{17}O^{18}O$ vs $\Delta^{18}O^{18}O$. Equilibrium curve contoured in T °C (Wang et al. 2004). Uncertainties are 0.17‰ for $\Delta^{18}O^{18}O$ and 0.3‰ for $\Delta^{17}O^{18}O$.

Figure 7: Perspective drawing of the Oxygen Evolving Complex (OEC) embedded in the protein Photosystem II. The OEC consists of 1 Ca, 4 Mn, 5 O atoms and 4 H_2O molecules. The Ca atom and 3 of the four Mn lie at opposite corners of a distorted cube, separated by oxygens O1, O2, and O3. A fourth Mn (Mn4A) dangles to one side of the cuboid coordinated to it by oxygens O4 and O5. Two H_2O, W1 and W2, are coordinated to the dangling Mn and two to Ca, W3 and W4. (Fig. 1d copied from Suga et al. 2015)

This is a preprint, the final version is subject to change, of the American Mineralogist (MSA)
Cite as Authors (Year) Title. American Mineralogist, in press.
DOI: http://dx.doi.org/10.2138/am-2018-6137

798 **Figures**

799

800

801

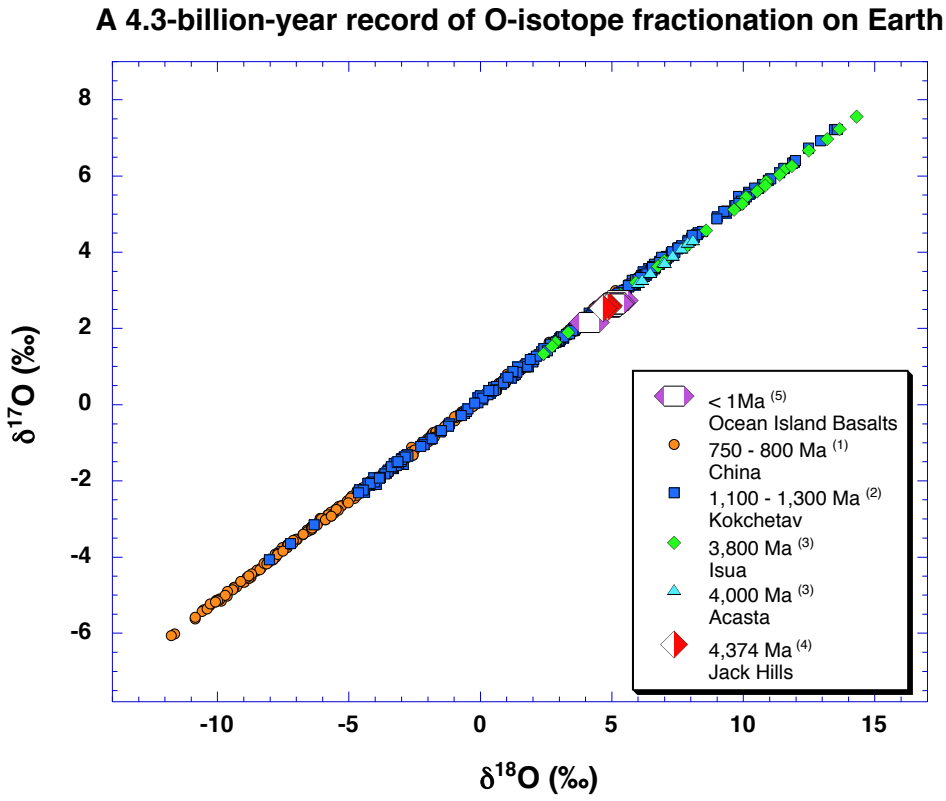

802

803 **Figure 1:** Plot of $\delta^{18}O$ vs. $\delta^{17}O$ showing Terrestrial Mass Fractionation Line (TFL) with
804 VSMOW as reference. The $\delta^{18}O$ vs. $\delta^{17}O$ values of planetary bodies such as Mars and 4 Vesta lie
805 on mass fractionation lines parallel to the TFL but offset above it (Mars) or below (4 Vesta, see
806 Figure 2B). Data: [1]Rumble & Yui, 1998; [2]Masago et al. 2003; [3]Rumble et al. 2013; [4]Valley et al.
807 2014; [5]Starkey et al. 2016. Uncertainties in $\delta^{18}O$ & $\delta^{17}O$ are approximately 0.1 ‰, smaller than
808 the plot symbols.

809

This is a preprint, the final version is subject to change, of the American Mineralogist (MSA)
Cite as Authors (Year) Title. American Mineralogist, in press.
DOI: http://dx.doi.org/10.2138/am-2018-6137

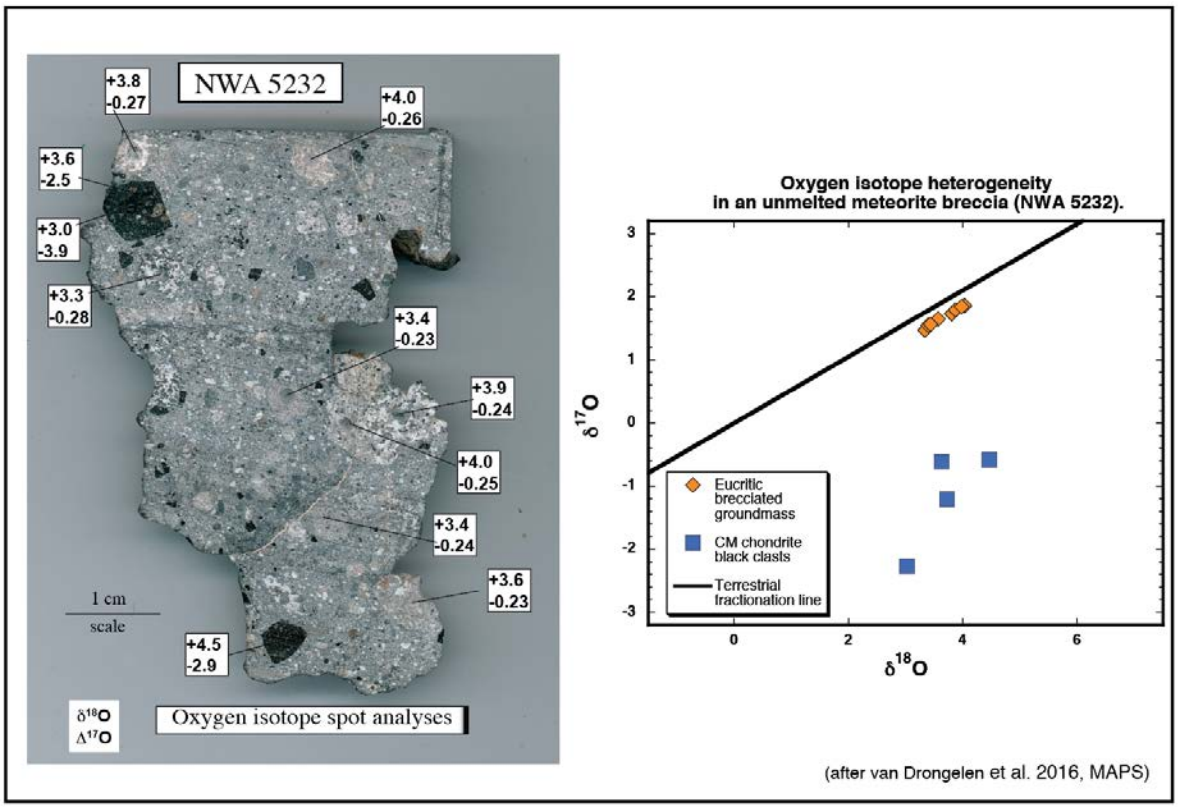

Figure 2: (A - left): Photograph of cut slab of meteorite NWA 5232 with $\delta^{18}O$ and $\Delta^{17}O$ values of spot analyses of CM chondrite clasts (black) and eucrite breccia fragments (gray) (van Drongelen et al. 2016). (B - right) $\delta^{18}O$ vs $\delta^{17}O$ plot of analyses of NWA 5232. The heavy black line is the TFL of Figure 1. Compare scattered distribution of data to linear array of Fig. 1. Uncertainties in $\delta^{18}O$ & $\delta^{17}O$ are approximately 0.1 ‰ and in $\Delta^{17}O$, 0.05 ‰.

This is a preprint, the final version is subject to change, of the American Mineralogist (MSA)
Cite as Authors (Year) Title. American Mineralogist, in press.
DOI: http://dx.doi.org/10.2138/am-2018-6137

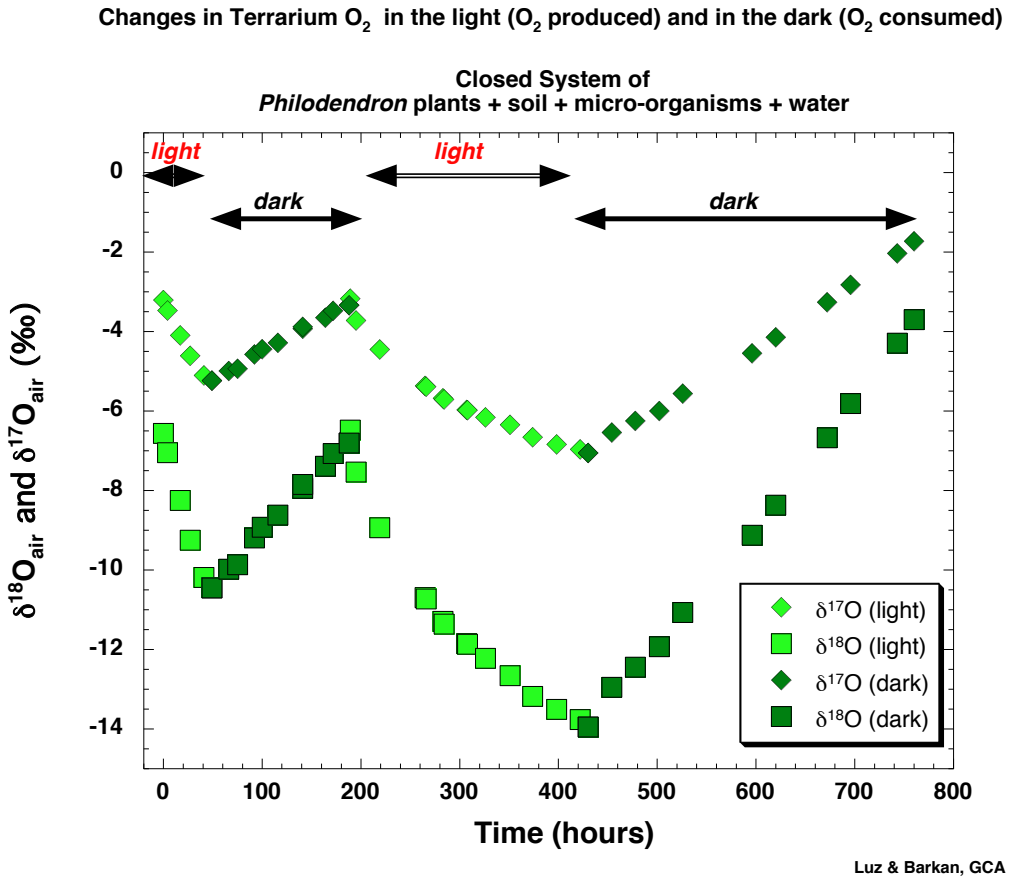

816

817 **Figure 3:** Plot of variations in $\delta^{17}O$, $\delta^{18}O$, and $\Delta^{17}O$ vs. time in atmosphere of closed
818 terrarium containing living *Philodendron,* soil, micro-organisns, and water. Note
819 distinctive variations in $\delta^{17}O$ and $\delta^{18}O$ in the light and in the dark (data replotted from
820 Luz and Barkan, 2005).

821

822

823

824

This is a preprint, the final version is subject to change, of the American Mineralogist (MSA)
Cite as Authors (Year) Title. American Mineralogist, in press.
DOI: http://dx.doi.org/10.2138/am-2018-6137

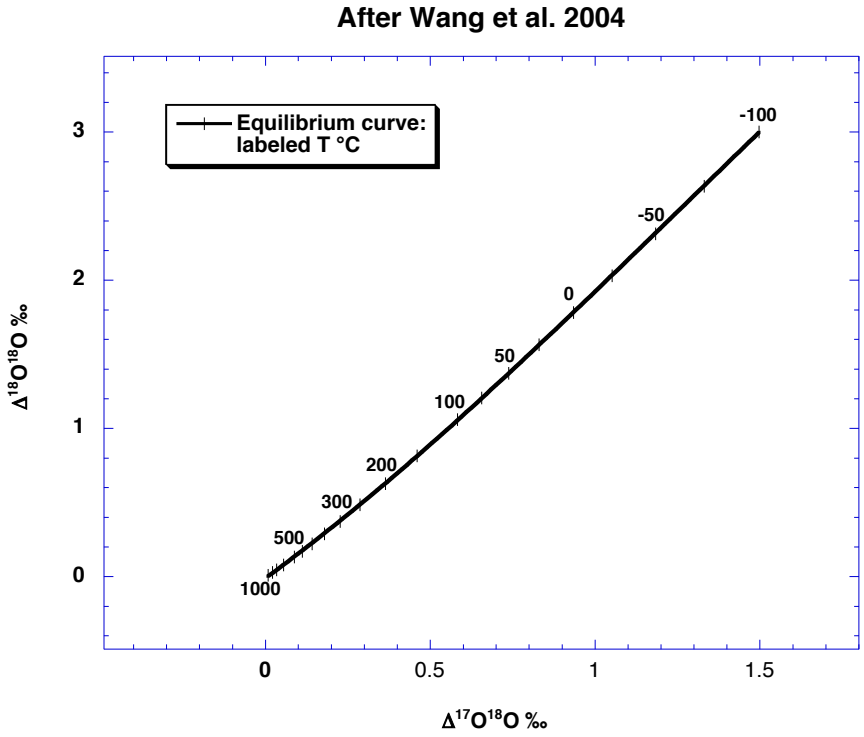

825

826 **Figure 4:** Plot of equilibrium curve for $\Delta^{17}O^{18}O$ (Δ_{35}) vs $\Delta^{18}O^{18}O$ (Δ_{36}) contoured in T °C (after

827 Wang et al. 2004). The two isotopologues are assumed to coexist in isotope exchange equilibrium

828 in the same sample of O_2 gas.

829

This is a preprint, the final version is subject to change, of the American Mineralogist (MSA)
Cite as Authors (Year) Title. American Mineralogist, in press.
DOI: http://dx.doi.org/10.2138/am-2018-6137

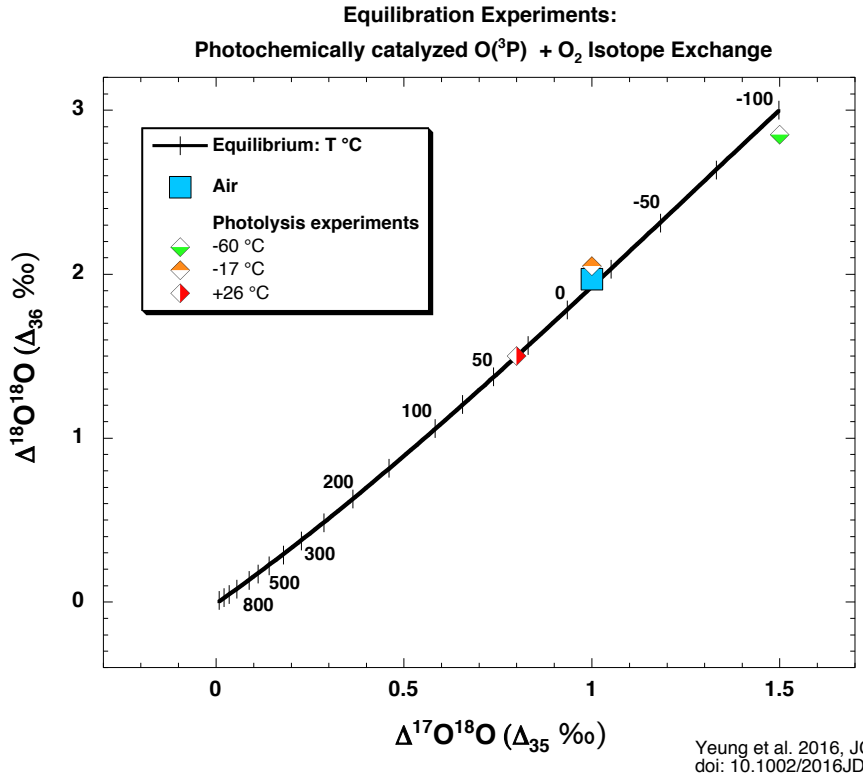

830

831 **Figure 5:** Plot of Δ_{35} (=$\Delta^{17}O^{18}O$) vs. Δ_{36} (= $\Delta^{18}O^{18}O$) for samples of O_2 gas subjected to

832 photolysis and $O(^3P)$ + O_2 catalysis. The plotted results demonstrate a tendency towards isotope

833 exchange equilibrium (Yeung et al. 2016). Uncertainties are 0.07‰ for $\Delta^{18}O^{18}O$ and 0.1‰ for

834 $\Delta^{17}O^{18}O$.

835

This is a preprint, the final version is subject to change, of the American Mineralogist (MSA)
Cite as Authors (Year) Title. American Mineralogist, in press.
DOI: http://dx.doi.org/10.2138/am-2018-6137

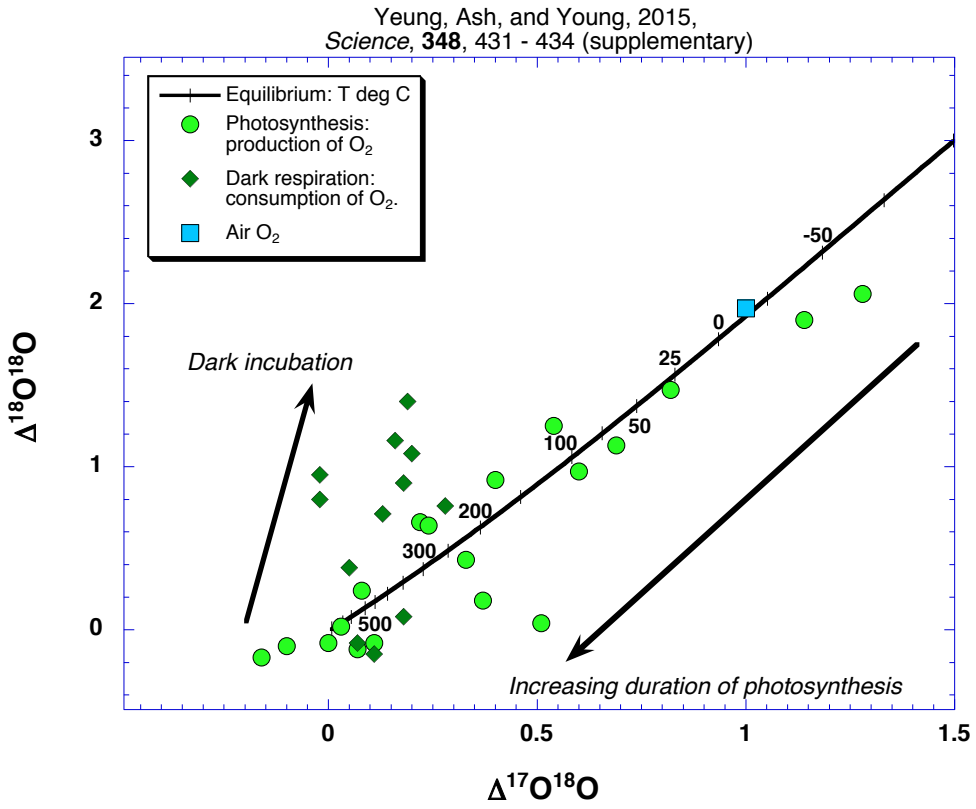

836

837 **Figure 6:** Plot of $\Delta^{17}O^{18}O$ vs $\Delta^{18}O^{18}O$ for oxygen produced during photosynthesis in the light and
838 residual O_2 remaining after plant respiration in the dark (Yeung et al. 2015, supplementary). The
839 values of $\Delta^{17}O^{18}O$ vs $\Delta^{18}O^{18}O$ decrease as long as photosynthesis in the light continues. Once the
840 light is extinguished, residual oxygen increases in $\Delta^{17}O^{18}O$ vs $\Delta^{18}O^{18}O$. Equilibrium curve
841 contoured in T °C (Wang et al. 2004). Uncertainties are 0.17‰ for $\Delta^{18}O^{18}O$ and 0.3‰ for
842 $\Delta^{17}O^{18}O$.

This is a preprint, the final version is subject to change, of the American Mineralogist (MSA)
Cite as Authors (Year) Title. American Mineralogist, in press.
DOI: http://dx.doi.org/10.2138/am-2018-6137

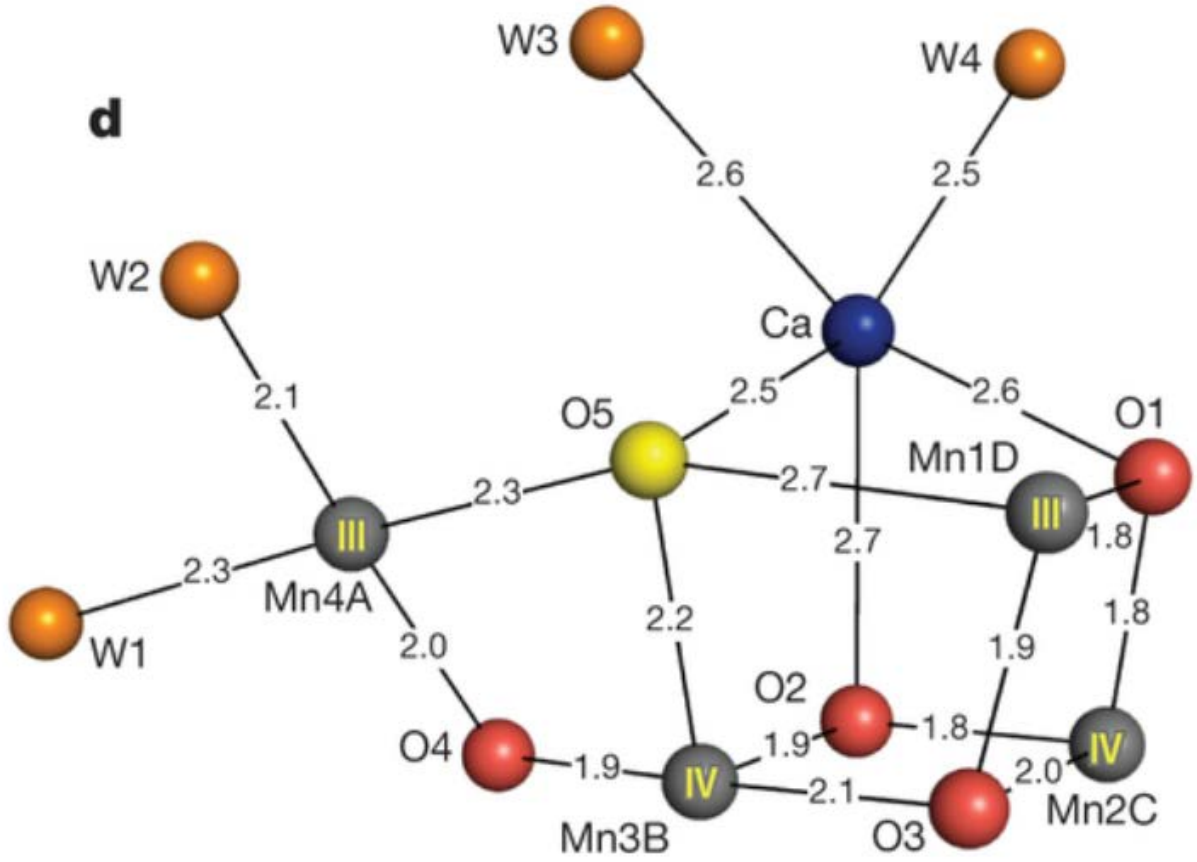

843
844

845

846 **Figure 7:** Perspective drawing of the Oxygen Evolving Complex (OEC) embedded in the protein
847 Photosystem II. The OEC consists of 1 Ca, 4 Mn, 5 O atoms and 4 H_2O molecules. The Ca atom
848 and 3 of the four Mn lie at opposite corners of a distorted cube, separated by oxygens O1, O2, and
849 O3. A fourth Mn (Mn4A) dangles to one side of the cuboid coordinated to it by oxygens O4 and
850 O5. Two H_2O, W1 and W2, are coordinated to the dangling Mn and two to Ca, W3 and W4.
851 (Fig. 1d copied from Suga et al. 2015)

852